applied sciences

MDPI

Article

Green Synthesis of a Cu/SiO_2 Catalyst for Efficient H_2-SCR of NO

Esteban Gioria [1], F. Albana Marchesini [1], Analía Soldati [2], Antonella Giorello [1], Jose L. Hueso [3,4,5,*] and Laura Gutierrez [1,*]

1 Institute of Research on Catalysis and Petrochemistry—INCAPE—(FIQ, UNL-CONICET)—Santiago del Estero 2829, Santa Fe 3000, Argentina; egioria.fiq@gmail.com (E.G.); albana.marchesini@gmail.com (A.M.); agiorello@santafe-conicet.gov.ar (A.G.)
2 Grupo de Caracterización de Materiales, Centro Atómico Bariloche, CONICET, Av. Bustillo 9500, S4140 San Carlos de Bariloche, PC S4140, Río Negro, Argentina; asoldati@cab.cnea.gov.ar
3 Institute of Nanoscience of Aragon (INA) and Department of Chemical Engineering and Environmental Technology, Edificio I+D+i, Campus Rio Ebro, University of Zaragoza, PC 50018 Zaragoza, Spain
4 Instituto de Ciencia de Materiales de Aragón (ICMA), Consejo Superior de Investigaciones Científicas (CSIC-Universidad de Zaragoza), PC 50018 Zaragoza, Spain
5 Networking Research Center on Bioengineering, Biomaterials and Nanomedicine (CIBER-BBN), 28029 Madrid, Spain
* Correspondence: jlhueso@unizar.es (J.L.H.); lbgutier@fiq.unl.edu.ar (L.G.)

Received: 22 July 2019; Accepted: 24 September 2019; Published: 29 September 2019

Featured Application: These catalysts can be envisioned for decontamination of nitrogen oxides from mobile and stationary exhaust sources.

Abstract: In this work, the synthesis of Cu/SiO_2 catalysts starting from pre-formed copper nanoparticle (CuNP) colloidal suspensions was carried out. Two different protocols for the CuNP synthesis were tested: (i) a green approach using water as solvent and ascorbic acid as reducer and stabilizing agent, and (ii) a second solvothermal method involving the use of diethylene glycol as solvent, sodium hypophosphite (NaH_2PO_2) as reducer, and polyvinylpyrrolidone (PVP) and cetyltrimethylammonium bromide (CTAB) as stabilizing agents. In addition, and for the sake of comparison, a third catalyst was prepared by solid state conventional grinding of CuO with SiO_2. The catalysts were tested in the environmentally relevant catalytic reduction of NO_X with H_2, in a temperature range from 300 to 500 °C. The catalysts were characterized by X-ray diffraction (XRD), temperature programmed reduction (TPR) cycles, Raman spectroscopy, and N_2 adsorption for specific surface BET measurements. From these techniques CuO and Cu(0) species were detected depending on the synthesis protocol. CuNP size and size distribution in the colloid suspensions were determined by transmission electronic microscopy (TEM). The catalyst prepared from the aqueous suspension ($CuAsc/SiO_2$) exhibited higher NO conversion (100%) and selectivity (85%) toward N_2 at the lower reaction evaluated temperature (300 °C). The $CuCTAB/SiO_2$ catalyst obtained by the solvothermal approach showed activity at high reaction temperature (400 °C) preferentially. The metal–support mechanical mixture exhibited a negligible response at low temperature and low conversion (68%) and selectivity (88%) at 500 °C. Nanoparticle size and distribution on the support, together with the metal–support interaction, were postulated as the most plausible parameters governing the catalytic performance of the different Cu/SiO_2 materials.

Keywords: copper nanoparticles; NO selective catalytic reduction; nanoparticle impregnation; copper–silica catalysts

1. Introduction

The emission of nitrogen oxides (NO_x, x = 1, 2) stemming from the combustion of fossil fuels in power plants or from the exhaust gases of mobile sources (i.e., road transport) is an ever-present environmental concern. These gases contribute to air pollution and lead to multiple environmental problems such as acid rain, photochemical smog, the greenhouse effect, among others [1,2]. Several alternatives for NO_x mitigation have been proposed. Since 1973, the selective catalytic reduction (SCR) of NO_x with ammonia (NH_3-SCR) has been widely utilized [3]. However, because of the risks associated with handling and storage of NH_3, NO_x reduction with hydrocarbon (HC) technology (HC-SCR) has been extensively studied [4]. There exist numerous works in the literature reporting the use of different hydrocarbons as reducing agents and a wide variety of catalysts under these reaction conditions [4,5]. While this approach looks very promising, it has not been extensively applied yet due to a series of drawbacks such as: (i) catalyst deactivation; (ii) limited selectivity of NO_x to N_2; (iii) high reaction temperatures, (iv) the need of excess HC that must be burnt, and finally (v) incremental air pollution (CO_2) and energy consumption.

Consequently, it is important to find methods for NO_x reduction that (i) reduce the CO_2 emissions, (ii) use green reducing agents, (iii) require lower energy costs, and (iv) involve low-cost, greener, active, selective and stable catalysts. In this regard, hydrogen has been considered to be a powerful alternative due to the fact that it is environmentally friendly and it forms H_2O and N_2 as the major end-products [6–9]. Equation (1) represents the overall reaction for the selective formation of N_2 using H_2 as reductant.

The studied catalytic systems for H_2-SCR are diverse and mostly based on the study of noble-metal catalysts [10]. For this reason, nowadays there is an increasing interest to develop alternative catalytic systems involving the use of less expensive and more abundant transition metals, with the respective economic benefits [11–15]. For instance, Pt supported on Al_2O_3 exhibits high activity for NO reduction. Nevertheless, the selectivity to N_2 decreases with increasing reaction temperatures [16–20]. In order to improve its catalytic performance, alternative supports have been systematically tested: SiO_2, TiO_2, MnO_x, and zeolites, together with perovskite type solids, etc. [21]. Pd and Ir deposited on different substrates have also been proposed as active materials towards NO_x H_2-SCR with a strong dependence of the final outcome on the metallic active site-support interactions and the specific reaction conditions [12]. Other catalysts based on noble metals such as Pd and Pt have shown better results even at low operating temperatures (below 200 °C) [6]. Nevertheless, the search for affordable and inexpensive catalysts based on non-noble transition metals increased the number of studies exploring the use of copper-based alternatives for the selective reduction of NO [22]. Bifunctional Cu–Al-MCM-41 catalysts were studied for both NO reduction and hydrocarbon oxidation [11]. The results showed that well dispersed and isolated Cu ions present in the mesoporous MCM-41 catalyst could act as an active redox center. Hence, hydrogen behaves as a better reducing agent than hydrocarbons, leading to an increased NO conversion at lower temperatures. The use of the Cu/ZSM-5 catalyst rendered a simple and straightforward NO reduction in the presence of hydrogen. However, the activity was almost negligible at reaction temperatures below 400 °C [23].

Regarding catalyst synthesis, the controlled deposition of a highly dispersed active phase onto a catalytic support has always been considered a challenging issue that strongly affects the final catalytic outcome. Conventional catalyst preparation methods are diverse, like wetness impregnation of metal precursors, co-precipitation, mechanical mixing, ionic exchange, and so on [24,25]. The advantages of these routes are well documented, and the synthesis of catalysts from a suspension of the active metal with nanometric size might turn out to be profitable [26–32]. Taking into account the synthesis of metal nanoparticles, there exists a large number of protocols that report the chemical reduction of the metallic precursor in solution as the most promising alternative approach [26,33,34].

In this work, two different protocols for the synthesis of colloidal copper nanoparticles (CuNPs) were developed. These pre-formed CuNPs were subsequently impregnated onto commercial silica Aerosil 300® supports. One of the selected CuNP protocol was carried out in a totally green aqueous

media, while the second one involved an organic medium with no eco-friendly reagents. Both Cu/SiO_2 catalysts obtained after the CuNP impregnation were evaluated and compared with a third catalyst obtained by solid state conventional grinding of CuO with SiO_2. The hydrogen-assisted reduction of NO was carried out as a test reaction to compare the catalytic behavior of the different materials in the 300–500 °C range.

2. Materials and Methods

2.1. Chemicals

Copper chloride ($CuCl_2 \cdot 2H_2O$, 99.0%, Sigma-Aldrich, CABA, Argentina) and copper sulphate ($CuSO_4 \cdot 5H_2O$, 98.0%, Sigma-Aldrich, CABA, Argentina) were used as metal precursors. Ascorbic acid ($C_6H_8O_6$, Cicarelli, 99.0%, Santa Fe, Argentina) was used as both green reductant and stabilizing agent. Sodium hypophosphite (NaH_2PO_2, Merck, 99.0%, Kenilworth, NJ, USA) was used as a reductant reagent, and polyvinylpyrrolidone ($(C_6H_9NO)_n$ PVP, K-30, Sigma-Aldrich, CABA, Argentina) together with cetyltrimethylammonium bromide ($C_{19}H_{42}BrN$, CTAB, 99.0%, Sigma-Aldrich, CABA, Argentina) were used as stabilizing agents. Water (Milli-Q grade) and diethylene glycol ($C_4H_{10}O_3$ Cicarelli, p.a. Santa Fe, Argentina) were used as solvents. Commercial silica Aerosil 300® was used as catalytic support.

All reagents were of analytical grade and were used as received without further purification.

2.2. Characterization Techniques

The quantitative chemical composition of the catalysts was performed by inductively coupled plasma atomic emission spectroscopy (ICP-AES) on an ICP-OPTIMA 2100 DV Perkin Elmer instrument. The particle size distribution was determined by transmission electronic microscopy (TEM) in a FEI Tecnai T-200 operated at 200 keV. Aberration corrected scanning transmission electron microscopy images for selected samples were acquired using a high angle annular dark field detector in a FEI XFEG TITAN electron microscope operated at 300 kV equipped with a CETCOR Cs-probe corrector from CEOS Company allowing formation of an electron probe of 0.08 nm. The geometric aberrations of the probe-forming system were controlled to allow a beam convergence of 24.7 mrad half-angle to be selected. Elemental analysis was carried out with an EDS (EDAX) detector, which allows EDX experiments to be performed in scanning mode. The samples were suspended in ethanol, under sonication, and 3 drops of each sample were carefully drop-casted onto Ni mesh grids. Specific surface area of the fresh and used catalysts were determined by N_2 adsorption isotherms and the BET equation was measured with the aid of an instrument Micromeritics Gemini V2.00-2380.

Fresh and used catalysts were additionally characterized by X-ray diffraction (DRX, Shimadzu model XD-D1 with a copper source radiation, CuKα). The Raman spectra were recorded using a LabRam spectrometer (Horiba-Jobin-Yvon) equipped with a CCD detector and a 532 nm excitation wavelength (laser power set at 30 mW) and a coupled Olympus confocal microscope.

Oxidation states of copper were determined by temperature programmed reduction experiments carried out up to 500 °C in H_2/Ar 5% v/v ambient, with a temperature heating ramp of 10 °C·min^{-1}. A Micromeritics AutoChem II-2920 equipment with a TCD detector was used for temperature programed reduction (TPR) analysis. The hydrogen consumption was referred in all cases to 50 mg of each dry sample placed in a U-shaped quartz tube reactor. The TPR profiles of the fresh samples were obtained after the calcination treatment, described in Section 2.3.2. For used samples, a first TPR (TPR-I) profile was performed. Then, after TPR-I, the same sample was re-oxidized in pure oxygen for 30 min at 500 °C and a second TPR (TPR-II) was obtained. All the TPR experiments were carried out by heating the samples at 10 °C·min^{-1} up to 500 °C in H_2/Ar 5% v/v flowing mixture.

Differential Scanning Calorimetry (DSC) was used to analyze the thermal decomposition of the unreacted precursors present in the catalysts. A Mettler Toledo instrument with a DSC821e module

was employed. Samples of 30–40 mg placed inside a 40 µL aluminum crucible were heated from 30 °C to 500 °C in air flow (50 $cm^3 \cdot min^{-1}$) employing a heating rate of 10 °C·min^{-1}.

2.3. Synthesis of Copper–Silica Catalysts

2.3.1. Synthesis of Copper Nanoparticles (CuNPs)

The greener synthesis route of CuNPs was inspired in a previous protocol reported by Xiong et al. [35] that combined the selection of copper chloride ($CuCl_2 \cdot 2H_2O$) as metal precursor (25 mL, 0.2 M) and ascorbic acid (25 mL, 1 M) as both reductant and stabilizing agent. The CuNP sample is referred to as CuAsc. Figure 1 shows the synthesis scheme and the suspension color evolution. The synthesis was carried out under refluxing conditions at 80 °C during 20 h of reaction employing water as solvent. The solution pH was not adjusted, reaching a value near to 3.

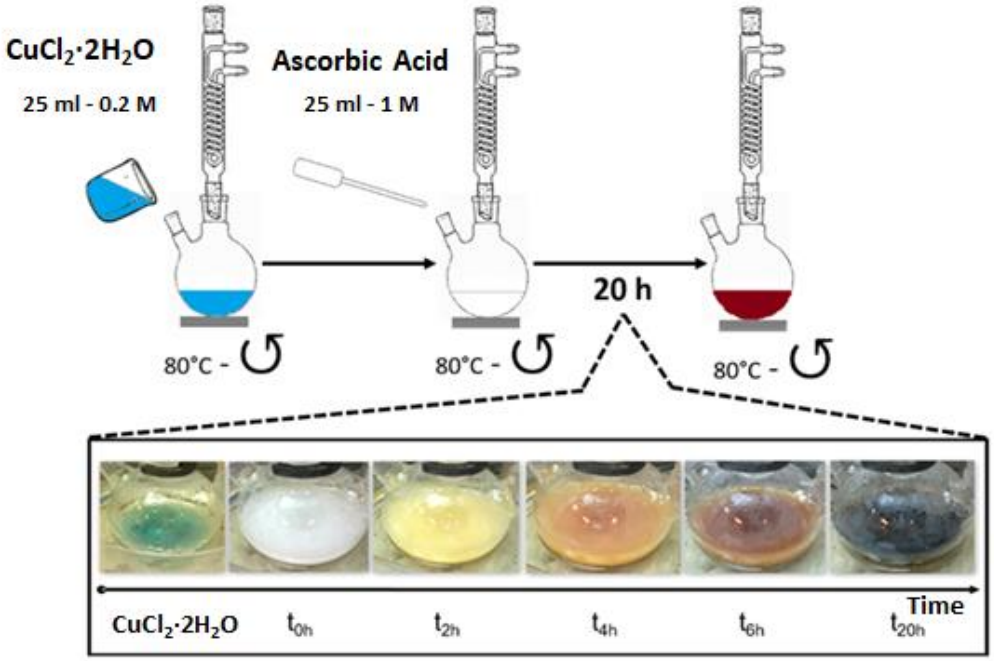

Figure 1. Scheme of the environmentally friendly protocol established to obtain CuNPs using water as solvent and ascorbic acid as mild reducing agent.

The second strategy to synthesize Cu colloidal NPs involved the use of a solvothermal synthesis approach previously proposed by Tang and co-workers [36]. This second protocol was conducted in diethylene glycol (DEG) as solvent, using cupric sulphate ($CuSO_4 \cdot 5H_2O$) as metallic precursor, sodium hypophosphite (NaH_2PO_2) as a reductant agent, and polyvinylpyrrolidone (PVP, K-30) together with cetyltrimethylammonium bromide (CTAB) as stabilizing agents. Figure 2 summarizes the different synthesis steps. The CuNPs obtained is referred to as CuCTAB. Three solutions were prepared: 25 mL of a solution of PVP/DEG (4% w/v) and CTAB/DEG (0.1 M), 25 mL of a solution (0.6 M) of NaH_2PO_2, and 50 mL of an aqueous solution of $CuSO_4 \cdot 5H_2O$ (0.2 M). Firstly, the solutions containing the reducing and stabilizing agents were mixed at 100 °C. Secondly, the solution with the metallic precursor was added at 140 °C (reaction temperature) and magnetically stirred for 5 min.

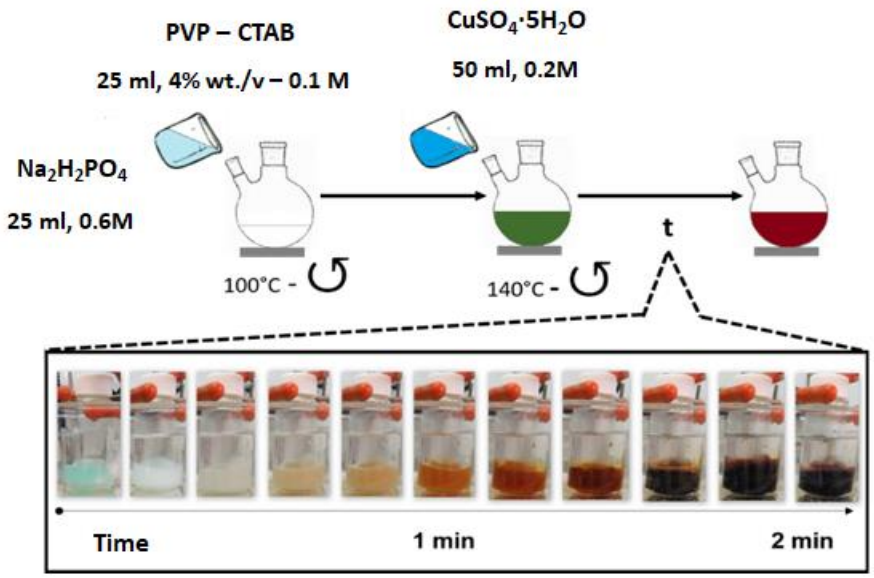

Figure 2. Schematic sequence of the different reaction steps in the solvothermal approach to obtain CuNPs using DEG as solvent.

2.3.2. Preparation of the Cu–SiO_2 Catalysts

The following step involved the wet impregnation of the preformed CuNPs on the SiO_2 support (Aerosil 300®) by wet impregnation of the CuNPs. Assuming a complete reduction of the copper precursors, a 4.2 mL aliquot of each resulting CuNP suspension was stirred in the presence of 500 mg of the support at 60 °C until ca. 90% of the liquid evaporated. Then, the catalysts were dried at 100 °C for 24 h in a conventional oven. The final metal loading was estimated in 1 wt.% by ICP analysis. The catalysts were labelled as CuAsc/SiO_2 and CuCTAB/SiO_2 depending on the protocol used in the CuNP preparation. For the sake of comparison, a third catalyst was prepared by conventional grinding of 495 mg of the silica support and 6.3 mg of copper (II) oxide. This catalyst was named CuOB/SiO_2. All solids were calcined in 100 mL·min^{-1} He/O_2 50% v/v conditions for 8 h at 500 °C, with a heating rate of 5 °C·min^{-1}. The synthetized catalysts were stored in a closed glass flask after calcination. Samples before and after catalytic evaluation were labeled as fresh and used, respectively.

2.4. Catalytic Reduction of NO with H_2

All catalysts prepared as described above were tested in a fixed bed reactor, using a gas hourly space velocity (GHSV) = 2250 h^{-1} defined as feed flow/catalytic bed volume. The catalytic tests were performed maintaining a constant copper content. The typical reacting mixture gases consisted of $[NO]_0$ = 2000 ppm, $[H_2]_0$ = 3% (v/v), balanced at 1 atm with He. The catalysts were pre-reduced at 400 °C in a 3% H_2 flow for 1 h. Before the catalytic tests, the solids were cooled to room temperature. Then, the catalytic activity was progressively measured at 300, 400, and 500 °C. The catalytic measurements were replicated three times for each catalyst with no significant variations on the final outcome (standard deviations below 5%). Every catalyst was kept under reaction conditions for at least six accumulated hours, not detecting any sign of deactivation in each fix reaction temperature interval of 2 h. The reactor effluent concentrations (ppm) of $[NO_x] = [NO] + [NO_2] + [N_2O]$, and $[NH_3]$ were monitored every 2 min with an on line FTIR Mattson Genesis II (resolution of 4 cm^{-1}) instrument equipped with a 15 cm path length gas IR cell with CaF_2 windows at RT. The N_2 production was calculated by atomic nitrogen balance. The NO conversion (C_{NO}, %) and the selectivity to N_2 (S, %) was calculated as follows:

$$C_{NO}\ (\%) = ([NO]_0 - [NO])/[NO]_0 * 100 \quad \text{(I)}$$

$$S\ (\%) = ([NO]_0 - [NO] - [NO_2] - 2[N_2O])/[NO]_0 * 100 \quad \text{(II)}$$

where [NO]0 is the initial concentration of NO (2000 ppm), whereas [NO], [NO_2] and [N_2O] are the concentrations of the corresponding components in the reactor effluent

3. Results and Discussion

3.1. Characterization of the Cu/SiO_2 Catalysts

Table 1 summarizes the CuNP particle sizes obtained by the different protocols and final metal loadings on the silica supports before and after the catalytic test, determined by ICP-AES. Quantitatively similar metal loadings were observed, for the fresh and used catalysts, confirming the absence of leaching phenomena under catalytic testing conditions. Figures S1 and S2 in Supplementary Materials show both TEM micrographs and histograms of the size distribution of copper nanoparticles before impregnation onto the silica. The CuCTAB/SiO_2 presented a turquoise–blue final color, while the CuOB/SiO_2 and CuAsc/SiO_2 resulted in brown solids (Figure S3 in Supplementary Materials).

Table 1. Particle size of the as prepared CuNPs and final Cu loading on the fresh and used catalysts.

CuNPs	Size (nm) [1]	Catalyst	Cu Loading (%) [2] Fresh Catalyst	Cu Loading (%) [2] Used Catalyst
CuO	-	CuOB/SiO_2	0.7 ± 0.1	0.7 ± 0.1
CuAsc	3.3 ± 0.9	CuAsc/SiO_2	0.9 ± 0.1	0.9 ± 0.1
CuCTAB	2.4 ± 0.7	CuCTAB/SiO_2	0.5 ± 0.1	0.5 ± 0.1

[1] Particle size measured by TEM micrographs, see Figures S1b and S2b in the Supplementary Materials. [2] Cu loading in the fresh catalysts, determined by ICP-AES.

The specific surface area and the N_2 adsorption isotherms of the fresh and used materials are detailed in Table 2 and Figure 3, respectively. Both CuOB/SiO_2 and CuCTAB/SiO_2 displayed an approximate decrease in specific surface area of 15%, with 12% losses observed for CuAsc/SiO_2. Consequently, the thermal process conducted during the catalytic tests did not significantly affect textural properties of the catalysts. This surface area reduction could be associated with partial sintering and intergrowth of a fraction of the spent CuAsc/SiO_2 catalyst, corroborated by STEM-EDX analysis

Table 2. Specific surface area data of fresh and used catalysts.

Specific Surface Area ($m^2.g^{-1}$)					
CuOB/SiO_2		CuAsc/SiO_2		CuCTAB/SiO_2	
Fresh [a]	Used [b]	Fresh [a]	Used [b]	Fresh [a]	Used [b]
280.4	230.4 (↓18) [c]	265.5	233.5 (↓12) [c]	275.3	239.2 (↓15) [c]

Specific surface area measurements: [a] fresh sample, after calcination treatment, [b] used samples, after the complete catalytic tests. [c] Specific surface area loss refers to the fresh sample.

DSC results (Figure S4 in the Supplementary Materials) showed that the organic components present in the CuNP suspensions (CuAsc and CuCTAB) were completely decomposed at the selected calcination temperature of 500 °C. X-ray diffraction analysis (Figure 4) of the calcined CuOB/SiO_2 catalyst revealed a CuO monoclinic structure of tenorite (2θ: 35.6° (111) and 38.7° (111) JCPDS 5-0661). In contrast, the same sample used under H_2-SCR NO_X reaction conditions showed the presence of metallic particles of Cu^0 (2θ: 43° (111) JCPDS 4-0836), thereby indicating that copper species remain reduced after being under reaction. Raman spectra (Figure S5, in Supplementary Materials) further confirmed that CuO species were present in both fresh and used catalysts due to the presence of Cu–O features at 300 and 350 cm^{-1} [37,38].

The XRD pattern of the calcined CuAsc/SiO_2 catalyst pointed out the presence of CuO moieties. However, after reaction, no copper species signals were distinguished in the corresponding diffractogram, but CuO could be observed by Raman spectroscopy. This could be due to the presence of particle sized smaller than the DRX instrument limit detection or that the species were amorphous

or atomically dispersed on the support [39]. No DRX patterns of copper species were detected for either fresh or used CuCTAB/SiO_2 catalysts. Nevertheless, CuO species could still be detected by Raman spectroscopy on the after-reaction sample (bands located at ca. 300 and 350 cm^{-1} in Figure S5 in Supplementary Materials) [40]. The fresh sample CuAsc/SiO_2 (not shown) also exhibited fluorescence under Raman measurement conditions [41].

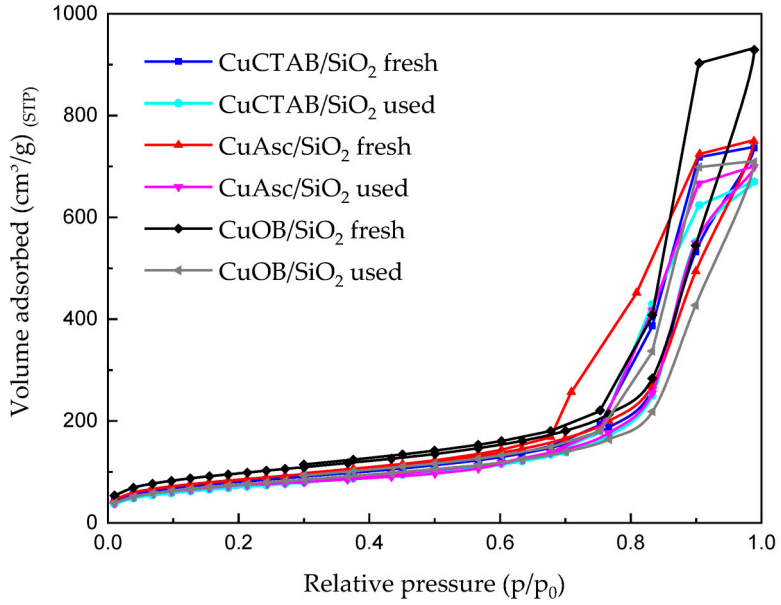

Figure 3. Nitrogen adsorption isotherms of the fresh and used catalysts.

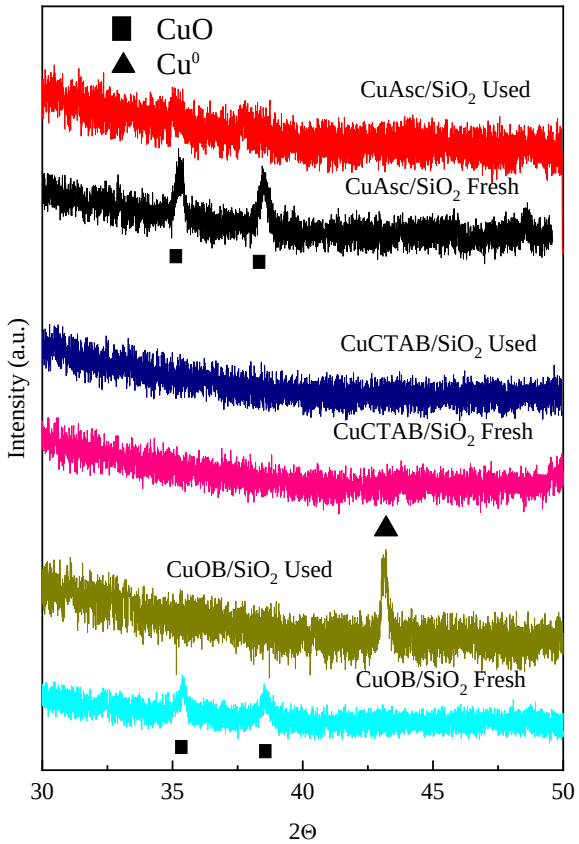

Figure 4. X-ray diffractograms of fresh and used catalysts.

Taking into account that the metal reducibility strongly depends on the particle size, oxidation state, and its interaction with the support [42–44], TPR analysis of the fresh Cu/SiO_2 catalysts was performed in order to obtain information about the nature of Cu species and their dispersion onto the support. Figure 5 and Table 3 show the TPR profiles and relative H_2 consumption, respectively. It could be noted that copper oxide was present in both $CuOB/SiO_2$ and $CuAsc/SiO_2$ calcined at 500 °C catalysts and that it was completely reduced at 400 °C. However, in the $CuCTAB/SiO_2$ sample an additional reduction effort (51%) was necessary at higher temperature, indicating that after the CuNPs were supported on SiO_2 49% of the copper remained as Cu(0).

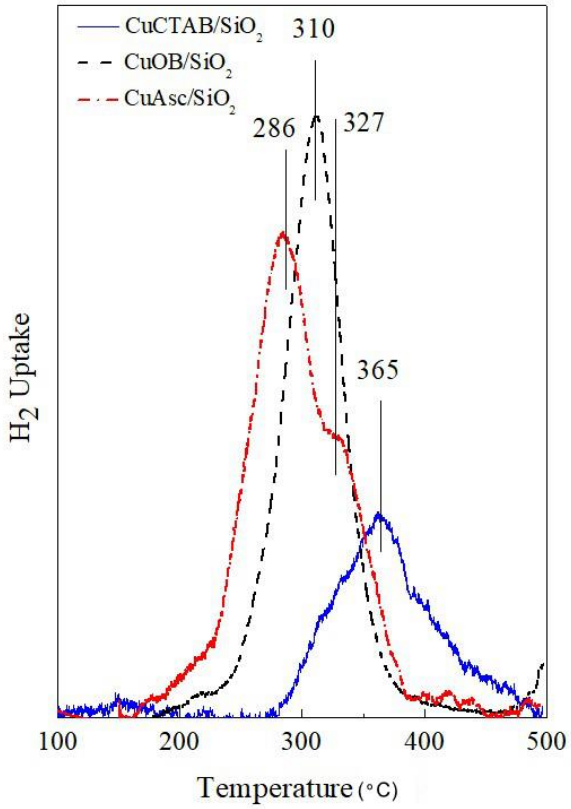

Figure 5. Temperature programmed reduction (TPR) profiles of the calcined fresh catalysts. Calcination treatment: 500 °C in air flow, heating rate: 10 °C min^{-1}. Solid line: $CuCTAB/SiO_2$, dash line: $CuOB/SiO_2$, dash dot line: $CuAsc/SiO_2$.

Table 3. Reducibility analysis of fresh, used, and re-oxidized catalysts.

Catalyst	H_2/Cu: Total Molar H_2 Consumption / Cu Molar Content			
	Fresh TPR-I	Fresh Re-Oxidized TPR-II	Used TPR-I	Used Re-Oxidized TPR-II
$CuOB/SiO_2$	1	-	0.06	1
$CuAsc/SiO_2$	1	-	0.65	1
$CuCTAB/SiO_2$	0.51	0.76	0.22	0.31

* TPR measurement conditions: H_2/Ar 5% v/v ambient, 30 mL·min^{-1}, heating ramp: 10 °C min^{-1} up to 500 °C, dry catalyst weight: 50 mg. The H_2 consumption was obtained taking into account the reduction of the CuO standard reagent under similar temperature programmed conditions.

Prior to the reaction tests, the catalysts were initially reduced at 400 °C in the presence of hydrogen. As a consequence, at the beginning of the reaction test, only metallic copper particles could be detected in the $CuOB/SiO_2$ and $CuAsc/SiO_2$ catalysts. In contrast, almost 50% of the copper was present as oxidized entities in the fresh $CuCTAB/SiO_2$ solid. The low reducibility of this sample may be attributed to (i) the presence of strong metal–support interaction that increased the reduction temperature of the

oxidized copper species, or (ii) the formation of silicalite type species during the calcination treatment evidenced by the turquoise–blue final color (Supplementary Materials Figure S3) [42,45]. The latter hypothesis could be sustained by the highly exothermic decomposition reaction during the calcination of the sample, which could generate high temperature spots leading to the formation of such Cu–Si complexes (Supplementary Materials Figure S4).

In order to verify the presence of metallic copper species and their interaction with SiO_2, the sample resulting from the TPR-I experiments was further calcined in air flow up to 500 °C. Then a subsequent H_2-TPR (TPR-II) was performed.

The TPR-I profile of the CuOB/SiO_2 catalyst after reaction indicated that the main copper species supported on SiO_2 was in metallic state Cu(0) (94%) (Figure 6A, Table 3). An analogous effect could be observed in the CuAsc/SiO_2 used catalyst with ca. 65% of reduced copper entities (Figure 6B). However, in the CuCTAB/SiO_2 catalysts, 22% of the initial CuO remained as Cu^{+n}. Not only the H_2 consumption was modified after all catalytic tests, but also the maximum reduction temperatures (Figure 6C). The H_2 uptake profiles of the used catalysts prepared from the CuNP suspensions shifted to lower temperatures. This could be attributed to a lower interaction of the CuO particles with the support or to the particle size changes on the support surface [46].

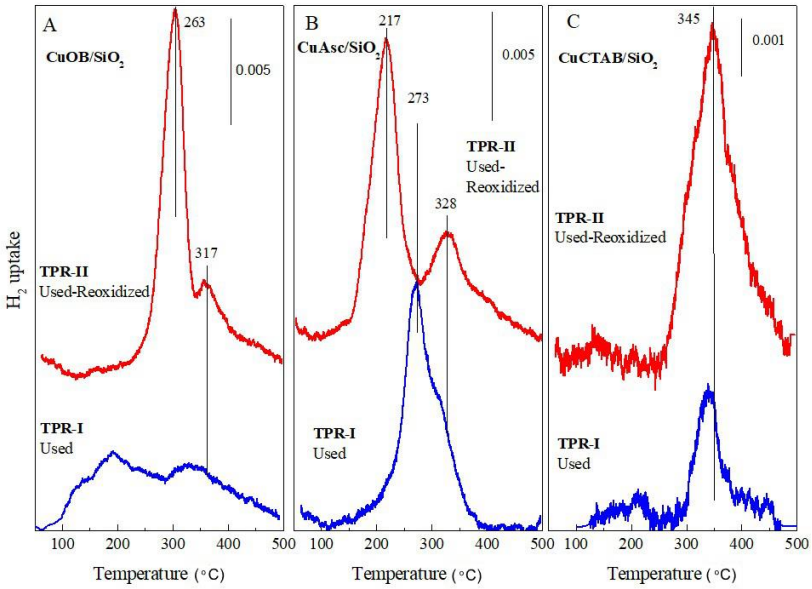

Figure 6. TPR profiles of the used (TPR-I) and re-oxidized catalysts after TPR-I (TPR-II). (**A**) CuOB/SiO_2, (**B**) CuAsc/SiO_2, (**C**) CuCTAB/SiO_2. Catalyst weight: 50 mg. Re-oxidation treatment: 500 °C in air flow, heating rate: 10 °C min^{-1}.

For the CuAsc/SiO_2 fresh catalyst, TPR-I revealed a maximum at 286 °C with a shoulder at 327 °C, which suggests the reduction of CuO in two different steps: Cu(II) to Cu(I) and Cu(I) to Cu(0), respectively) [46]. However, this former peak could be also associated with particles with different sizes [47]. It could be observed that at 400 °C all copper species were reduced.

Regarding the CuCTAB/SiO_2 catalyst, the TPR profile of the fresh catalyst (Figure 5C) showed a main peak around 365 °C with a shoulder at 441 °C. A second TPR after re-oxidation (not shown) showed a 20% increment in the H_2 consumption higher than in the fresh catalyst, thereby suggesting that part of the copper remained in the metallic state even after being supported and calcined or that Cu–Si like entities formed during the pretreatment were less prone to reduction. The TPR-I profile of the used solid CuOB/SiO_2 catalyst (Figure 6A) showed that H_2 consumption decreased notably, suggesting that after the reaction a great percentage of the metal remained reduced [44]. After this TPR-I, the sample was re-oxidized up to 500 °C during 30 min under pure oxygen flow, and a new TPR-II was obtained. In this second profile two peaks appeared, one at 263 °C and other at 317 °C,

confirming that after reaction, copper particles did not oxidize completely and probably the dispersion of the same ones changed over the support [47–49].

For the CuAsc/SiO_2 used catalyst, a similar profile was observed that resembled the calcined sample, but with a lower H_2 consumption. This indicates that a fraction of copper remained as metallic particles (Cu(0)), in agreement with the XRD pattern (Figure 4). The profile of the used and re-oxidized catalyst (TPR-II, Figure 6B) revealed two well-defined peaks (217 and 328 °C) whose H_2 consumption corresponded to the total reduction of copper (Table 3). These differences suggest that the oxidation treatment promoted some reorganization of copper species, which gave rise to two well defined reduction peaks at lower temperatures, indicating an increment of the reducibility of the sites and a decreasing metal–support interaction [50,51].

In the case of the CuCTAB/SiO_2 after reaction, the reduction area (Figure 6C) turned out to be much lower with a single peak centered at 340 °C. This suggests that a fraction of the copper particles remained like Cu(0) after the reaction. On the other hand, the total reduction of the copper entities took place at higher temperatures (350 °C) than the other catalytic counterparts (CuOB/SiO_2 and CuAsc/SiO_2). Consequently, it is possible to infer that the lower reducibility of this catalyst was due to a higher metal–support interaction. Moreover, it could be associated with the formation of a chrysocolla type phase, a kind of copper hydrosilicate [39,45,52].

From the evaluation of our Cu/SiO_2 catalysts by transmission electron microscopy (TEM) (Figures S6 and S7) it could infer the amorphous and nanometric morphology of the silica selected as support. For the grinded CuOB/SiO_2, both fresh and used, large CuO particle aggregates were mainly detected. In contrast, for both CuAsc/SiO_2 fresh and used it was not possible to discriminate individual CuNPs (Figures 7 and 8), indicating a very good dispersion of the preformed CuO_x nanoparticles within the SiO_2 support except for certain fractions of aggregated particles in the spent catalyst (Figure 8). In the case of the fresh CuCTAB/SiO_2 sample, a similar morphology to CuAsc/SiO_2 was observed. Nevertheless, the CuCTAB/SiO_2 sample after reaction revealed the presence of embedded CuNPs with higher average sizes. This could be associated with the formation of a silica–copper compound with high interaction that, after contact with reaction gases, formed small and strongly attached nanoparticles on the support.

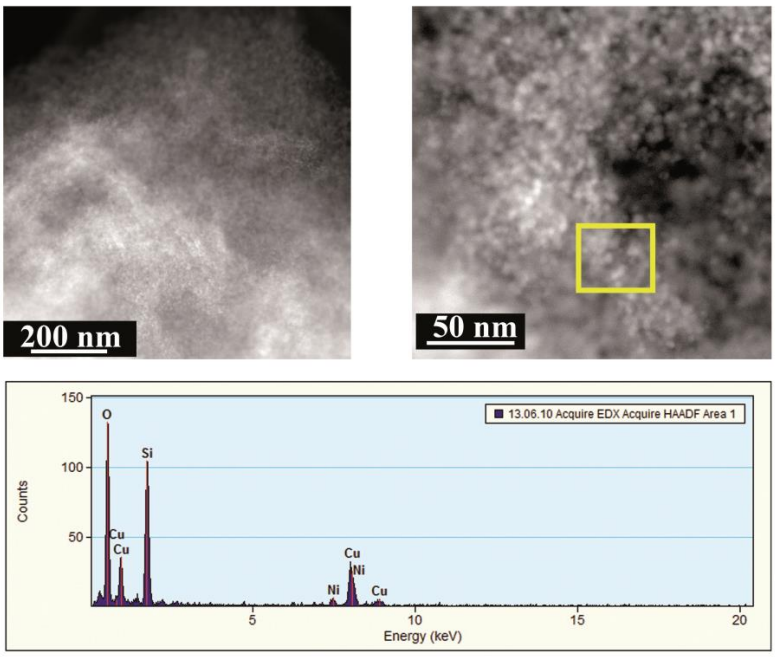

Figure 7. HAADF STEM images of the fresh CuAsc/SiO_2 catalyst and representative EDX spectrum of a selected area.

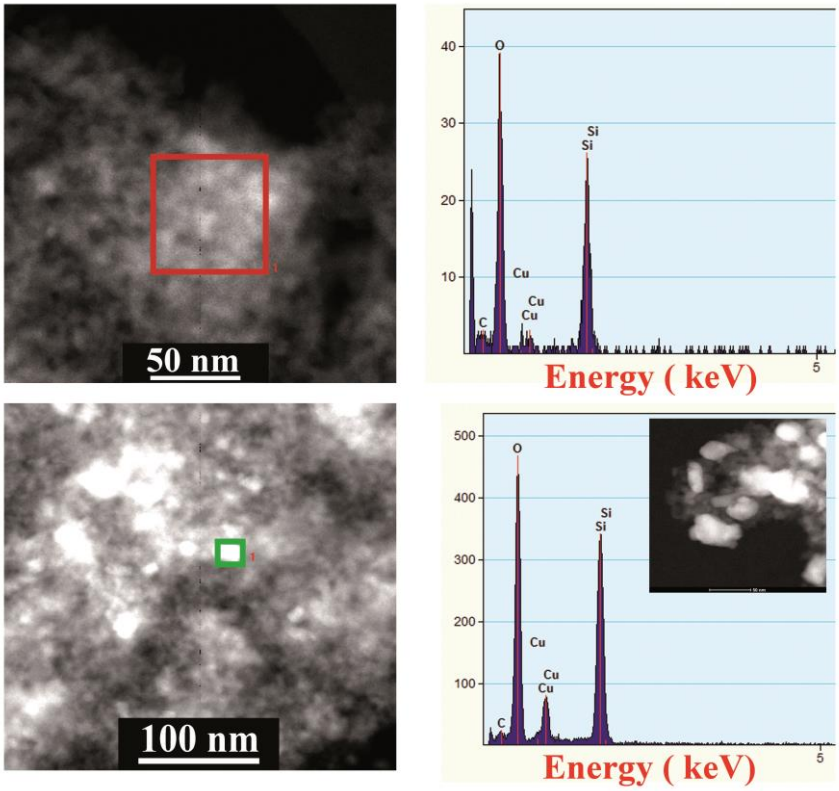

Figure 8. HAADF STEM images of the CuAsc/SiO_2 catalyst after reaction and representative EDX spectrum of a selected area.

3.2. Catalytic Evaluation in the NO Reduction with Hydrogen

The catalytic measurements were carried out in triplicate for each catalyst. No significant differences were found, thereby confirming a good reproducibility of the materials and the robustness of the methodology (Table 4). Although no long-term stability studies were conducted, all the catalysts exhibited stable NO conversion levels at each specific reaction temperature under evaluation for an accumulated experiment of six consecutive hours (two hours at 300 °C, two hours at 400 °C, and then two additional hours at 500 °C, respectively; see Figure 9 for comparison) Regarding the activity of the solid mixture CuOB/SiO_2 catalyst, Figure 9A and Table 4 show the conversion of NO in the presence of H_2. Total NO conversion was not observed at any evaluated temperature and total selectivity towards N_2 solely was achieved at 400 °C, at the expense of lower NO conversion levels. Nevertheless, the activity of this material was negligible at 300 °C for the reduction with H_2. Figure 9B and Table 4 also summarize the catalytic performance of the CuAsc/SiO_2. In this case, the NO conversion was total for the full temperature ranges. At 500 °C the reduction reaction showed N_2 and NO_2 as the main products presenting selectivity to N_2, of 88%, whereas at 400 °C only N_2 was formed. It is worth highlighting that the catalyst showed activity at 300 °C with an outstanding 86% of selectivity to nitrogen.

Table 4. NO conversion and NO to N_2 selectivity from the catalytic tests [1].

Catalyst	Total NO Conversion C_{NO} (%) [2]			NO to N_2 Selectivity S_{N2} (%) [3]		
	300 °C	400 °C	500 °C	300 °C	400 °C	500 °C
CuOB/SiO_2	0	75 ± 1	68 ± 1	0	75 ± 1	88 ± 1
CuAsc/SiO_2	100	100	100	85 ± 1	100	88 ± 1
CuCTAB/SiO_2	0	100	100	0	100	100

[1] Reaction conditions: $[NO]_0$ = 2000 ppm NO, $[H_2]_0$ = 3% H_2, balanced at 1 atm with He, GHSV: 2250 h^{-1}. [2] Equation (I). [3] Equation (II). Minimal deviations were obtained in the catalytic tests (triplicates).

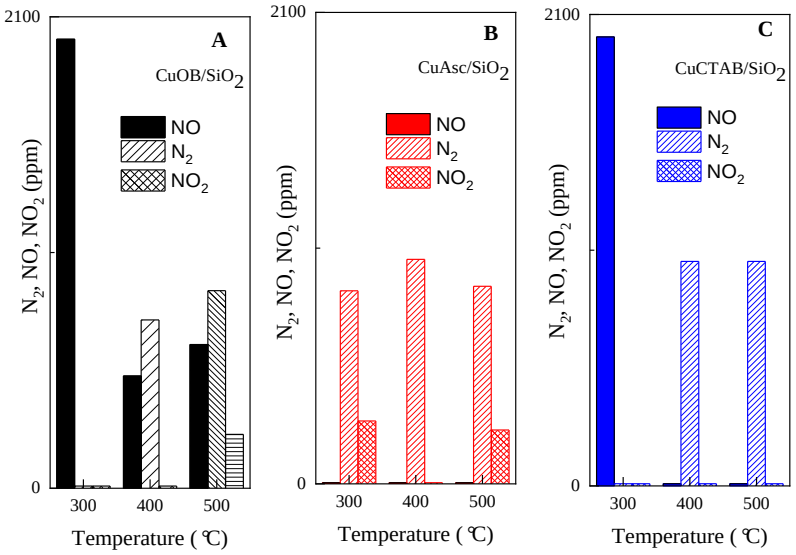

Figure 9. Catalytic activity of A: $CuOB/SiO_2$, B: $CuAsc/SiO_2$, and C: $CuCTAB/SiO_2$ for the NO reduction with H_2. Reaction conditions: $[NO]_0$ = 2000 ppm NO, $[H_2]_0$ = 3% H_2, balanced at 1 atm with He, GHSV: 2250 h^{-1}.

Concerning the catalytic activity of $CuCTAB/SiO_2$, both the conversion of NO and the selectivity towards N_2 was 100% at temperatures of 400 °C and 500 °C, respectively (Figure 9C and Table 4), while no reaction occurred at lower reaction temperatures of 300 °C.

These results clearly indicate that each catalyst presented different copper species interacting particularly with the support and with a specific dispersion that led to distinct catalytic performance.

The following reactions could take place between NO and H_2 [53–56].

$$NO + H_2 \rightarrow \frac{1}{2} N_2 + H_2O \quad (1)$$

$$2\,NO + 5\,H_2 \rightarrow 2\,NH_3 + 2\,H_2O \quad (2)$$

$$4\,NO \rightarrow N_2 + 2\,NO_2 \quad (3)$$

$$2\,NO + H_2 \rightarrow N_2O + H_2O \quad (4)$$

$$2\,NO + H_2 \rightarrow N_2O + H_2O \quad (5)$$

The only end-products observed in the catalytic reaction with all the prepared solids were NO, N_2, NO_2, and H_2O. Neither NH_3 nor N_2O were detected as reaction products, as it was observed when the test was performed with the support (SiO_2) without copper at the same reaction conditions. This result indicated the selective role of the copper towards nitrogen regardless of the reaction temperature. A simple redox cycle for the selective reduction of NO with H_2 was proposed as a catalytic mechanism, as seen in Figure 10 [23]:

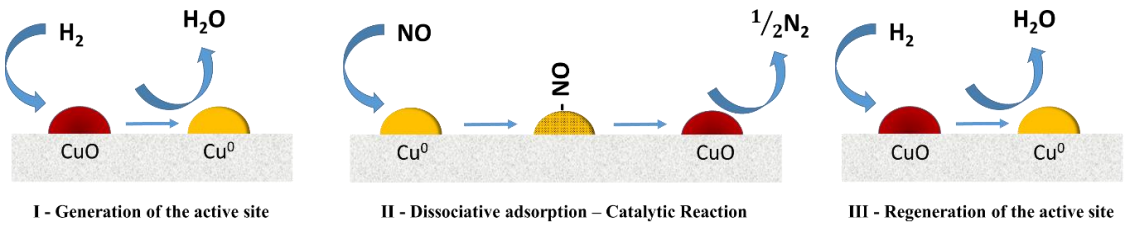

Figure 10. Simple redox cycle for the selective reduction of NO with H_2.

In this redox cycle, metallic copper is formed under reductant atmosphere forming the active site. Nitrogen oxide is adsorbed and dissociated, forming nitrogen and copper oxide on the catalyst. In a final step, this oxidized site is regenerated under a reducing atmosphere.

The presence of NO_2 could be associated with a labile Cu–O surface species that contributes to a fast NO oxidation [57]. This mechanism agrees with the behavior exhibited by the studied catalysts. On the other hand, previous studies of CuO reduction with H_2 by in-situ XRD claimed that under analogous experimental conditions, CuO was directly reduced into Cu^0 without the formation of intermediate oxides such as Cu_2O or Cu_4O_3 [58,59]. Likewise, the same authors studied the effect of the oxidation of metallic copper in similar conditions used in this report. Their results demonstrated that despite the fact that Cu_2O is a stable intermediate oxide, only CuO was present at the end of the treatment. These results are in agreement with the information revealed by XRD and Raman spectroscopy of our fresh and used catalysts with no clear evidence for the presence of intermediate oxides (Figure 4 and Figure S5 in Supplementary Materials). This would indicate that the active site is metallic copper, remaining as CuO or Cu–O adsorbed species after reaction. Additionally, NO_2 formation for CuAsc/SiO_2 at 300 and 500 °C, and for CuOB/SiO_2 at 500 °C could be associated with the adsorption of NO on the oxidized copper sites (see Figure 10). Then, in a second step, the reduction to metallic copper regenerates the active site with the subsequent oxidation of NO and release of NO_2 [23].

4. Conclusions

Copper–silica catalysts synthesized from pre-formed Cu nanoparticles have shown a promising response towards the selective reduction of nitrogen oxides. The use of greener and more environmentally friendly reactants rendered the best results in terms of NO conversion levels and selectivity to N_2 even at reaction temperatures below 300 °C. The use of preformed colloidal CuNPs seems very promising and convenient to establish a good dispersion of the metallic active sites. The results were more remarkable for the CuNPs retrieved from greener precursors that rendered activity and selectivity at milder reaction temperatures than the catalysts prepared by solid state grinding or by solvothermal approaches. The lack of a good homogeneity, the absence of a good metal–support interaction, and the potential interference of organics were the main causes attributed to the different performances of the probed catalysts. The fact that the catalysts prepared following the greener protocol were active and selective towards NO reduction even at lower reaction demonstrates the advantage of the proposed preparation method. The dispersion of the copper species, particle size on the support, and its degree of interaction with the same one notably affected the catalytic activity. In the sample prepared by mechanical mixing, the size of particles would limit the activity of the catalyst. In the case of the catalyst prepared from CuNPs suspended in organic solvent, a high interaction metal/support would work to weaken activity to the active site.

Supplementary Materials: The following are available online at http://www.mdpi.com/2076-3417/9/19/4075/s1. Figure S1. Representative TEM image and particle size distribution of Cu nanoparticles synthesized with ascorbic acid (CuAsc NPs); Figure S2. Representative TEM image and particle size distribution of Cu nanoparticles retrieved from the solvothermal approach using CTABr (CuCTAB NPs); Figure S3. Digital photographs of the resulting Cu/SiO_2 fresh catalysts: a) CuAsc/SiO_2; b) CuCTAB/SiO_2; c) CuOB/SiO_2 (physical mixture); Figure S4: Study of decomposition of the CuNP precursors during the calcination of the catalysts calcination by Differential Scanning Calorimetry (DSC). Sample weight: 30–40 mg, Air flowing rate: 50 mL min^{-1}, Heating rate of 10 °C min^{-1}; Figure S5. Raman spectra corresponding to the fresh and spent Cu/SiO_2 catalysts; Figure S6. Transmission electron microscopy images of the different fresh Cu/SiO_2 catalysts: (a,b) Cu/SiO_2 obtained by solid mixture; (c,d) Cu/SiO_2 obtained by the impregnation of pre-formed CuNPs retrieved through the greener approach with ascorbic acid; (e,f) Cu/SiO_2 obtained by the impregnation of pre-formed CuNPs retrieved through the solvothermal approach using CTABr and organic chemicals; Figure S7. Transmission electron microscopy images of the different Cu/SiO_2 catalysts after H_2-SCR NO reaction: (a–b) Cu/SiO_2 obtained by solid mixture; (c–d) Cu/SiO_2 obtained by the impregnation of pre-formed CuNPs retrieved through the greener approach with ascorbic acid; (e–f) Cu/SiO_2 obtained by the impregnation of pre-formed CuNPs retrieved through the solvothermal approach using CTABr and organic chemicals.

Author Contributions: Conceptualization, E.G. and L.G.; Data curation, E.G., F.A.M., A.S., L.G., and J.L.H.; Formal analysis: E.G., A.S., and L.G.; Funding acquisition, L.G. and J.L.H.; Investigation, E.G. and L.G.; Methodology, E.G., A.G., L.G., and J.L.H.; Project administration, L.G.; Resources, L.G.; Supervision, L.G.; Validation, E.G.; Visualization, J.L.H.; Writing—original draft, E.G., F.A.M., and L.G.; Writing—review and editing, E.G., L.G., and J.L.H.

Funding: The authors wish to acknowledge the financial support received from ANPCyT (PICT/16-2284), CONICET (PIP/14-406), and UNL (CAID+D-2016-50420150100037LI), and to the Agencia Santafesina de Ciencia, Tecnología e Innovación (ASACTEI 2010-038-16, Res 121/16). Esteban Gioria also wants to thank the Santa Fe Bank Foundation for the partial financing of this work within the student grant "Technological Innovation 2014". Part of this work was funded by Gobierno de Aragón (T57_17R p) and cofunded by Feder 2014–2020 "Construyendo Europa desde Aragón". Financial support from the European Research Council Advanced Grant (HECTOR-267626), the Spanish Government (MINECO-PRI-PIBAR-2011-1366), and the Regional Government of Aragon (DGA) is gratefully acknowledged. The synthesis of materials was performed by the Platform of Production of Biomaterials and Nanoparticles of the NANOBIOSIS ICTS, more specifically by the Nanoparticle Synthesis Unit of the CIBER in BioEngineering, Biomaterials, and Nanomedicine (CIBER-BBN).

Acknowledgments: Thanks are also given to Guillermina Amrein for the English language editing.

Conflicts of Interest: The authors declare no conflict of interest.

References

1. Brookshear, D.W.; Pihl, J.A.; Toops, T.J.; West, B.; Prikhodko, V. The selective catalytic reduction of NOx over Ag/Al_2O_3 with isobutanol as the reductant. *Catal. Today* **2016**, *267*, 65–75. [CrossRef]
2. Ji, Y.; Bai, S.; Crocker, M. Al_2O_3-based passive NO_x adsorbers for low temperature applications. *Appl. Catal. B Environ.* **2015**, *170–171*, 283–292. [CrossRef]
3. Lai, J.K.; Wachs, I.E. A Perspective on the Selective Catalytic Reduction (SCR) of NO with NH3 by Supported $V2O_5$-WO_3/TiO_2 Catalysts. *ACS Catal.* **2018**, *8*, 6537–6551. [CrossRef]
4. Brandenberger, S.; Kröcher, O.; Tissler, A.; Althoff, R. The state of the art in selective catalytic reduction of NO_x by ammonia using metal-exchanged zeolite catalysts. *J. Catal. Rev.* **2008**, *50*, 492–531. [CrossRef]
5. Fu, M.; Li, C.; Lu, P.; Qu, L.; Zhang, M.; Zhou, Y.; Yu, M.; Fang, Y. A review on selective catalytic reduction of NO_x by supported catalysts at 100–300°C—Catalysts, mechanism, kinetics. *Catal. Sci. Technol.* **2014**, *4*, 14–25. [CrossRef]
6. Resitoglu, I.A.; Keskin, A. Hydrogen applications in selective catalytic reduction of NO_x emissions from diesel engines. *Int. J. Hydrogen Energy* **2017**, *42*, 23389–23394. [CrossRef]
7. Zhao, X.; Zhang, X.; Xu, Y.; Liu, Y.; Wang, X.; Yu, Q. The effect of H_2O on the H_2-SCR of NO_xover Pt/HZSM-5. *J. Mol. Catal. A Chem.* **2015**, *400*, 147–153. [CrossRef]
8. Yadav, D.; Singh, P.; Prasad, R. $MnCo_2O_4$ spinel catalysts synthesized by nanocasting method followed by different calcination routes for low-temperature reduction of NO_x using various reductants. *Int. J. Hydrogen Energy* **2018**, *43*, 5346–5357. [CrossRef]
9. Costa, C.N.; Savva, P.G.; Fierro, J.L.G.; Efstathiou, A.M. Industrial H_2-SCR of NO on a novel Pt/MgO-CeO_2 catalyst. *Appl. Catal. B Environ.* **2007**, *75*, 147–156. [CrossRef]
10. Burch, R.; Coleman, M.D. An investigation of the $NO/H_2/O_2$ reaction on noble-metal catalysts at low temperatures under lean-burn conditions. *Appl. Catal. B Environ.* **1999**, *23*, 115–121. [CrossRef]
11. Karthik, M.; Bai, H. Selective catalytic reduction of NO using acetone solvent vapors as the reducing agent over Cu^{2+} and/or Al^{3+}ions substituted MCM-41 catalysts. *Appl. Catal. B Environ.* **2014**, *144*, 809–815. [CrossRef]
12. Li, J.; Wu, G.; Guan, N.; Li, L. NO selective reduction by hydrogen over bimetallic Pd-Ir/TiO_2 catalyst. *Catal. Commun.* **2012**, *24*, 38–43. [CrossRef]
13. Abu-jrai, A.; Tsolakis, A.; Megaritis, A. The influence of H_2 and CO on diesel engine combustion characteristics, exhaust gas emissions, and after treatment selective catalytic NO_x reduction. *Int. J. Hydrogen Energy* **2007**, *32*, 3565–3571. [CrossRef]
14. Hueso, J.L.; Cotrino, J.; Caballero, A.; Espinós, J.P.; González-Elipe, A.R. Plasma catalysis with perovskite-type catalysts for the removal of NO and CH_4 from combustion exhausts. *J. Catal.* **2007**, *247*, 288–297. [CrossRef]
15. Caballero, A.; Morales, J.J.; Cordon, A.M.; Holgado, J.P.; Espinos, J.P.; Gonzalez-Elipe, A.R. An in situ XAS study of Cu/ZrO_2 catalysts under de-NO_x reaction conditions. *J. Catal.* **2005**, *235*, 295–301. [CrossRef]

16. Caravaggio, G.; Nossova, L.; Burich, R. Influence of Supports on Pd Catalysts for the Selective Catalytic Reduction of NO_x with H_2 and CO. *Emiss. Control Sci. Technol.* **2016**, *2*, 10–19. [CrossRef]
17. Schott, F.J.P.; Balle, P.; Adler, J.; Kureti, S. Reduction of NO_x by H_2 on $Pt/WO_3/ZrO_2$ catalysts in oxygen-rich exhaust. *Appl. Catal. B Environ.* **2009**, *87*, 18–29. [CrossRef]
18. Wang, L.; Yin, C.; Yang, R.T. Selective catalytic reduction of nitric oxide with hydrogen on supported Pd: Enhancement by hydrogen spillover. *Appl. Catal. A Gen.* **2016**, *514*, 35–42. [CrossRef]
19. Breen, J.P.; Burch, R.; Hill, C.J. NO_x storage during H_2 assisted selective catalytic reduction of NO_x reaction over a Ag/Al_2O_3 catalyst. *Catal. Today* **2009**, *145*, 34–37. [CrossRef]
20. Huai, L.Y.; Wang, H.; He, C.Z.; Wen, H.; Yi, W.C.; Liu, J.Y. Effect of Subsurface Oxygen on Selective Catalytic Reduction of NO by H_2 on Pt(100): A First-Principles Study. *J. Phys. Chem. C* **2015**, *119*, 24819–24826. [CrossRef]
21. Liu, Z.; Li, J.; Woo, S.I. Recent advances in the selective catalytic reduction of NO_x by hydrogen in the presence of oxygen. *Energy Environ. Sci.* **2012**, *5*, 8799–8814. [CrossRef]
22. Pereda-Ayo, B.; De La Torre, U.; Illán-Gómez, M.J.; Bueno-López, A.; González-Velasco, J.R. Role of the different copper species on the activity of Cu/zeolite catalysts for SCR of NO_x with NH. *Appl. Catal. B Environ.* **2014**, *147*, 420–428. [CrossRef]
23. Burch, R.; Scire, S. An investigation of the mechanism of the selective catalytic reduction of NO on various metal/ZSM-5 catalysts: Reactions of H_2/NO mixtures. *Catal. Lett.* **1994**, *27*, 177–186. [CrossRef]
24. Schwarz, J.A.; Contescu, C.; Contescu, A. Methods for Preparation of Catalytic Materials. *Chem. Rev.* **1995**, *95*, 477–510. [CrossRef]
25. Pinna, F. Supported metal catalysts preparation. *Catal. Today* **1998**, *41*, 129–137. [CrossRef]
26. Ojha, N.K.; Zyryanov, G.V.; Majee, A.; Charushin, V.N.; Chupakhin, O.N.; Santra, S. Copper nanoparticles as inexpensive and efficient catalyst: A valuable contribution in organic synthesis. *Coord. Chem. Rev.* **2017**, *353*, 1–57. [CrossRef]
27. Bhuyan, D.; Saikia, M.; Saikia, L. ZnO nanoparticles embedded in SBA-15 as an efficient heterogeneous catalyst for the synthesis of dihydropyrimidinones via Biginelli condensation reaction. *Microporous Mesoporous Mater.* **2018**, *256*, 39–48. [CrossRef]
28. Seth, J.; Nepak, D.; Chaudhari, V.R.; Prasad, B.L.V. Preparation of MgO supported platinum nanoparticle catalyst using toluene dispersed platinum sol. *Appl. Surf. Sci.* **2017**, *418*, 87–91. [CrossRef]
29. Peng, R.; Li, S.; Sun, X.; Ren, Q.; Chen, L.; Fu, M.; Wu, J.; Ye, D. Size effect of Pt nanoparticles on the catalytic oxidation of toluene over Pt/CeO2 catalysts. *Appl. Catal. B Environ.* **2018**, *220*, 462–470. [CrossRef]
30. Zaccheria, F.; Scotti, N.; Marelli, M.; Psaro, R.; Ravasio, N. Unravelling the properties of supported copper oxide: Can the particle size induce acidic behaviour? *Dalton Trans.* **2013**, *42*, 1319–1328. [CrossRef]
31. Miguel-Sancho, N.; Martinez, G.; Sebastian, V.; Malumbres, A.; Florea, I.; Arenal, R.; Ortega-Liebana, M.C.; Hueso, J.L.; Santamaria, J. Pumping Metallic Nanoparticles with Spatial Precision within Magnetic Mesoporous Platforms: 3D Characterization and Catalytic Application. *ACS Appl. Mater. Interfaces* **2017**, *9*, 41529–41536. [CrossRef] [PubMed]
32. Usón, L.; Colmenares, M.G.; Hueso, J.L.; Sebastián, V.; Balas, F.; Arruebo, M.; Santamaría, J. VOCs abatement using thick eggshell Pt/SBA-15 pellets with hierarchical porosity. *Catal. Today* **2014**, *227*, 179–186. [CrossRef]
33. Karthik, A.D.; Geetha, K. Synthesis of copper precursor, copper and its oxide nanoparticles by green chemical reduction method and its antimicrobial activity. *J. Appl. Pharm. Sci.* **2013**, *3*, 16–21.
34. Karthikeyan, S.; Kumar, S.; Durndell, L.J.; Isaacs, M.A.; Parlett, C.M.A.; Coulson, B.; Douthwaite, R.E.; Jiang, Z.; Wilson, K.; Lee, A.F. Size-Dependent Visible Light Photocatalytic Performance of Cu_2O Nanocubes. *ChemCatChem* **2018**, *10*, 3554–3563. [CrossRef]
35. Xiong, J.; Wang, Y.; Xue, Q.; Wu, X. Synthesis of highly stable dispersions of nanosized copper particles using l-ascorbic acid. *Green Chem.* **2011**, *13*, 900–904. [CrossRef]
36. Tang, X.F.; Yang, Z.G.; Wang, W.J. A simple way of preparing high-concentration and high-purity nano copper colloid for conductive ink in inkjet printing technology. *Colloids Surf. A Physicochem. Eng. Asp.* **2010**, *360*, 99–104. [CrossRef]
37. Tsoncheva, T.; Issa, G.; Blasco, T.; Dimitrov, M.; Popova, M.; Hernández, S.; Kovacheva, D.; Atanasova, G.; Nieto, J.M.L. Catalytic VOCs elimination over copper and cerium oxide modified mesoporous SBA-15 silica. *Appl. Catal. A Gen.* **2013**, *453*, 1–12. [CrossRef]

38. Perez-Robles, F.; Garcia-Rodriguez, F.J.; Jimenez-Sandoval, S.; Gonzalez-Hernandez, J. Raman study of copper and iron oxide particles embedded in an SiO_2 matrix. *J. Raman Spectrosc.* **1999**, *30*, 1099–1104. [CrossRef]
39. Amiri, T.Y.; Moghaddas, J. Cogeled copperesilica aerogel as a catalyst in hydrogen production from methanol steam reforming. *Int. J. Hydrogen Energy* **2015**, *40*, 1472–1480. [CrossRef]
40. Balamurugan, B.; Mehta, B.R.; Avasthi, D.K.; Singh, F.; Arora, A.K.; Rajalakshmi, M.; Raghavan, G.; Tyagi, A.K.; Shivaprasad, S.M. Modifying the nanocrystalline characteristics—Structure, size, and surface states of copper oxide thin films by high-energy heavy-ion irradiation. *J. Appl. Phys.* **2002**, *92*, 3304–3310. [CrossRef]
41. Wang, Z.; Chen, B.; Rogach, A.L. Synthesis, optical properties and applications of light-emitting copper nanoclusters. *Nanoscale Horizons* **2017**, *2*, 135–146. [CrossRef]
42. Huang, Z.; Cui, F.; Kang, H.; Chen, J. Highly dispersed silica-supported copper nanoparticles prepared by precipitation—Gel method: A simple but efficient and stable catalyst for glycerol hydrogenolysis. *Chem. Mater.* **2008**, *20*, 5090–5099. [CrossRef]
43. Chen, L.F.; Guo, P.J.; Qiao, M.H.; Yan, S.R.; Li, H.X.; Shen, W.; Xu, H.L.; Fan, K.N. Cu/SiO_2 catalysts prepared by the ammonia-evaporation method: Texture, structure, and catalytic performance in hydrogenation of dimethyl oxalate to ethylene glycol. *J. Catal.* **2008**, *257*, 172–180. [CrossRef]
44. Marchi, A.J.; Fierro, J.L.G.; Santamaría, J.; Monzón, A. Dehydrogenation of isopropylic alcohol on a Cu/SiO2catalyst: A study of the activity evolution and reactivation of the catalyst. *Appl. Catal. A Gen.* **1996**, *142*, 375–386. [CrossRef]
45. Kirichenko, O.; Kapustin, G.; Nissenbaum, V.; Strelkova, A.; Shuvalova, E.; Shesterkina, A.; Kustov, L. Thermal decomposition and reducibility of silica-supported precursors of Cu, Fe and Cu–Fe nanoparticles. *J. Therm. Anal. Calorim.* **2018**, *134*, 233–251. [CrossRef]
46. Gallo, A.; Tsoncheva, T.; Marelli, M.; Mihaylov, M.; Dimitrov, M.; Dal Santo, V.; Hadjiivanov, K. Size controlled copper nanoparticles hosted in mesoporous silica matrix: Preparation and characterization. *Appl. Catal. B Environ.* **2012**, *126*, 161–171. [CrossRef]
47. Guerreiro, E.D.; Gorriz, O.F.; Rivarola, J.B.; Arrúa, L.A. Characterization of Cu/SiO_2 catalysts prepared by ion exchange for methanol dehydrogenation. *Appl. Catal. A Gen.* **1997**, *165*, 259–271. [CrossRef]
48. Gentry, S.J.; Walsh, P.T. Influence of silica and alumina supports on the temperature-programmed reduction of copper(II) oxide. *Faraday Trans.* **1982**, *13*, 1515–1523. [CrossRef]
49. Wang, Z.; Liu, Q.; Yu, J.; Wu, T.; Wang, G. Surface structure and catalytic behavior of silica-supported copper catalysts prepared by impregnation and sol-gel methods. *Appl. Catal. A Gen.* **2003**, *239*, 87–94. [CrossRef]
50. Tu, C.H.; Wang, A.Q.; Zheng, M.Y.; Wang, X.D.; Zhang, T. Factors influencing the catalytic activity of SBA-15-supported copper nanoparticles in CO oxidation. *Appl. Catal. A Gen.* **2006**, *297*, 40–47. [CrossRef]
51. Van Der Grift, C.J.G.; Mulder, A.; Geus, J.W. Characterization of silica-supported copper catalysts by means of temperature-programmed reduction. *Appl. Catal.* **1990**, *60*, 181–192. [CrossRef]
52. Spassova, I.; Stoeva, N.; Nickolov, R.; Atanasova, G.; Khristova, M. Impact of carbon on the surface and activity of silica-carbon supported copper catalysts for reduction of nitrogen oxides. *Appl. Surf. Sci.* **2016**, *369*, 120–129. [CrossRef]
53. Nguyen, L.; Zhang, S.; Wang, L.; Li, Y.; Yoshida, H.; Patlolla, A.; Takeda, S.; Frenkel, A.I.; Tao, F. Reduction of Nitric Oxide with Hydrogen on Catalysts of Singly Dispersed Bimetallic Sites Pt 1 Co m and Pd 1 Co n. *ACS Catal.* **2016**, *6*, 840–850. [CrossRef]
54. Ueda, A.; Haruta, M. Nitric Oxide Reduction with Hydrogen, Carbon Monoxide, and Hydrocarbons over Gold Catalysts. *Gold Bull.* **2011**, *32*, 3–11. [CrossRef]
55. Shelef, M.; Gandhi, H.S. Ammonia Formation in Catalytic Reduction of Nitric Oxide by Molecular Hydrogen. II. Noble Metal Catalysts. *Ind. Eng. Chem. Prod. Res. Dev.* **1972**, *11*, 393–396. [CrossRef]
56. Ueda, A.; Nakao, T.; Azuma, M.; Kobayashi, T. Two conversion maxima at 373 and 573 K in the reduction of nitrogen monoxide with hydrogen over Pd/TiO_2 catalyst. *Catal. Today* **1998**, *45*, 135–138. [CrossRef]
57. López-Suárez, F.E.; Bueno-López, A.; Illán-Gómez, M.J. Cu/Al_2O_3 catalysts for soot oxidation: Copper loading effect. *Appl. Catal. B Environ.* **2008**, *84*, 651–658. [CrossRef]

58. Rodriguez, J.A.; Kim, J.Y.; Hanson, J.C.; Pérez, M.; Frenkel, A.I. Reduction of CuO in H_2: In situ time-resolved XRD studies. *Catal. Lett.* **2003**, *85*, 247–254. [CrossRef]
59. Kim, J.Y.; Rodriguez, A.; Hanson, J.C.; Frenkel, A.I.; Lee, P.L. Reduction of CuO and Cu_2O with H_2: H Embedding and kinetic effects in the formation of suboxides. *J. Am. Chem. Soc.* **2003**, *125*, 10684–10692. [CrossRef]